Electronic Supplementary Material (ESI) for New Journal of Chemistry.

REVISED

Design, Synthesis, and Structural Evaluation of Metal Complexes of Azepane-1-carbodithioate for Targeting Human Breast Cancer: Investigating Cytotoxic Activity against MDA-MB-231 Cell Line

Shubham Jaiswal[a], Nilesh Rai[b], Suryansh Chandra[a], Ashish Verma[b], Vibhav Gautam[b], Manu Adhikari[c] Sanjay Singh[c], M.K. Bharty[a],

[a]*Department of Chemistry, Banaras Hindu University, Varanasi-221005, India*

[b]*Centre of Experimental Medicine and Surgery, Institute of Medical Sciences, Banaras Hindu University, Varanasi-221005, India*

[c]*Department of Chemical Sciences, Indian Institute of Science Education and Research Mohali, Knowledge City, Sector 81, Mohali-140306, India*

*Corresponding author email: manoj_vns2005@yahoo.co.in; mkbharty@bhu.ac.in

Contents

1. Materials and Methods:

1.1 Chemical and starting materials

Commercial reagents were used without further purification and all the experiments were carried out in the open atmosphere and at room temperature. The starting material Hexamethyleneimine (Azepane) was purchased from Sigma Aldrich. The solvents were dried and distilled before their use.

1.2 Physical measurements

Infrared spectra were recorded in the region of 400-4000 cm^{-1}as KBr pellets on a Varian Excalibur 3100 FT-IR spectrophotometer. ^{1}H and ^{13}C NMR spectra were recorded in $CDCl_3$ on a JEOL JNM-ECZ500R/S1 FT-NMR spectrometer using TMS as an internal reference. Electronic spectra were recorded at different solution concentrations in $CDCl_3$ on a SIMADZU 1700 UV-vis. spectrophotometer and emissions spectra were recorded on Agilent Technologies Cary Eclipsed Fluorescence Spectrophotometer. Magnetic susceptibility measurements were conducted at room temperature using a Cahn–Faraday electrobalance, with $Hg[Co(NCS)_4]$ serving as the calibrant.

2. Anti-cancer study

2.1 Cell viability Assay

MTT assay was employed to check the cytotoxicity of the synthesized ligands and complexes [1-5]. In brief, cells (1×10^4 cells/well) were grown in 96-well plates and treated with varying concentrations of the ligand and complexes, and kept for overnight in a humidified CO_2 incubator at 37 °C. Following incubation, MTT solution (5 mg/mL) was applied to each well and the plate was placed in a CO_2 incubator for 3h. The absorbance of the solubilized crystals was measured at 595 nm on a microplate using a microplate reader (Thermo Scientific, multiskan FC) only after the insoluble formazan crystal was dissolved in 100 µL DMSO. GraphPad Prism 5 software was used to calculate the IC_{50} values using the given equation:

$$\%\ Cell\ Viability = \frac{Absorbance\ in\ the\ treated\ group}{Absorbance\ in\ the\ untreated\ group} x100$$

2.2 Cell Proliferation Assay

MDA-MB 231 (5 x 10^3 cells/well) cells were treated with 10 µg/mL of ligand and its metal complexes for 24h and 0.1% DMSO (vehicle control) [6]. The culture medium was removed and cells were fixed with ethanol for 10 min. Afterward, crystal violet solution (0.05% crystal violet in 20% ethanol) was added for 10 min. The cells were washed with running tap water and crystals were solubilized with methanol. Absorbance at 595 nm was measured using a microplate reader, and the triplicate values were plotted on a graph.

2.3 Quantification of glucose in cell culture supernatant

The glucose level of the cell-free culture supernatant was quantified by a commercial glucose estimation kit (Beacon Diagnostics, India) following the manufacturer's protocol [7]. Concisely, MDA-MB-231 (1x 10^5 cells/well) were treated with respective IC_{50} concentrations of ligand and metal complexes and kept in CO_2 incubator for 24 h of incubation period. Afterward, 10 µL of culture supernatant was taken from each treatment group and mixed with 1 mL of working reagent containing phenol, glucose-oxidase, peroxidase, and 4-aminoantipyrine followed by incubation at 37 °C for 10 min. The absorbance of the reaction mixture was taken at 492 nm using a microplate reader. The concentration of glucose was expressed in mg/dL.

2.4 Nitrite estimation assay in cell culture supernatant

The level of nitric oxide (NO) was estimated by indirectly measuring the nitrite (NO_2) (one of the stable breakdown products of NO) level following the method described by Ding *et al*. [8], with a slight modification based on the Griess reaction. The Griess Reagent system is based on the two-step diazotization reaction that converts nitrite into an azo dye product by using sulphanilamide and naphthyl-ethylene diamine dihydrochloride (NED) under acidic conditions (phosphoric acid), which can be quantified spectrophotometrically at 540 nm. Briefly, culture supernatant was incubated with an equal volume of Griess reagent [1% (*w/v*) sulfanilamide in 2.5% H_3PO_4 and 0.1% (*w/v*) naphthyl-ethylene diamine dihydrochloride] and

kept in dark at room temperature for 10 min in a 96-well culture plate. The absorbance was taken at 540 nm using a microplate reader.

3. IR Spectra of Ligand and its Complexes

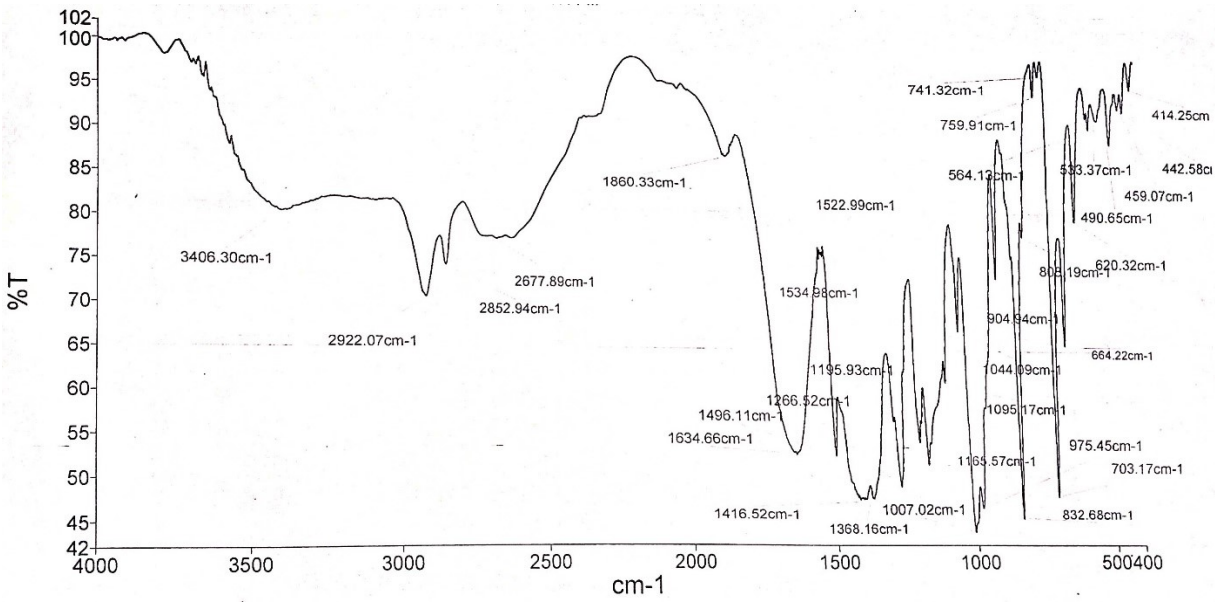

Supplementary Fig. 1: IR spectrum of ligand

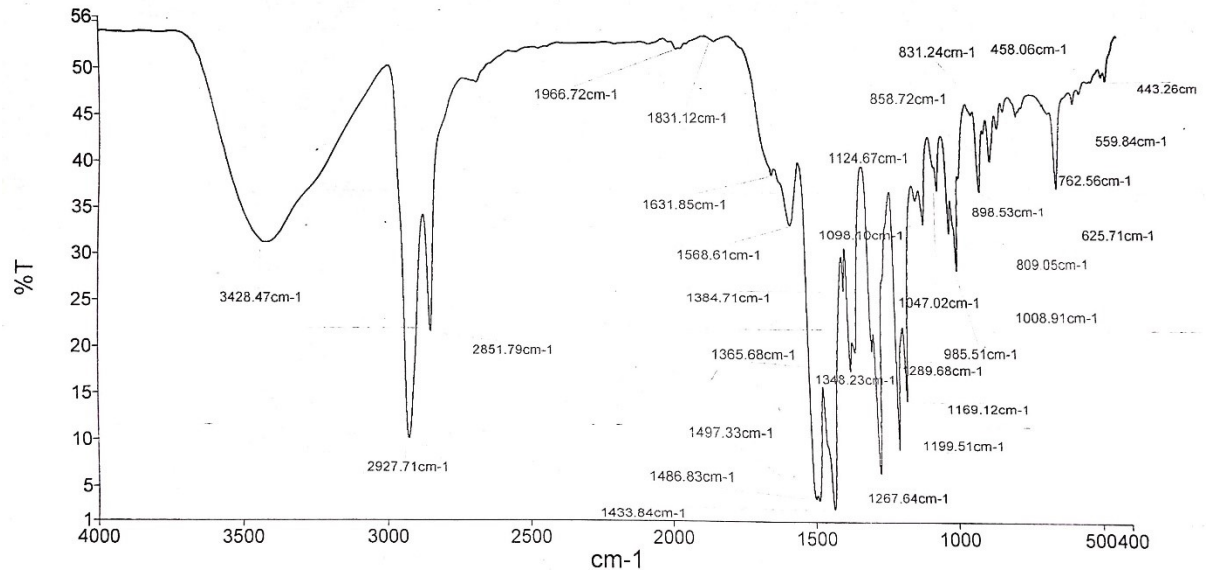

Supplementary Fig. 2: IR spectrum of $[Co(acdt)_3]\cdot CHCl_3$ (**1**)

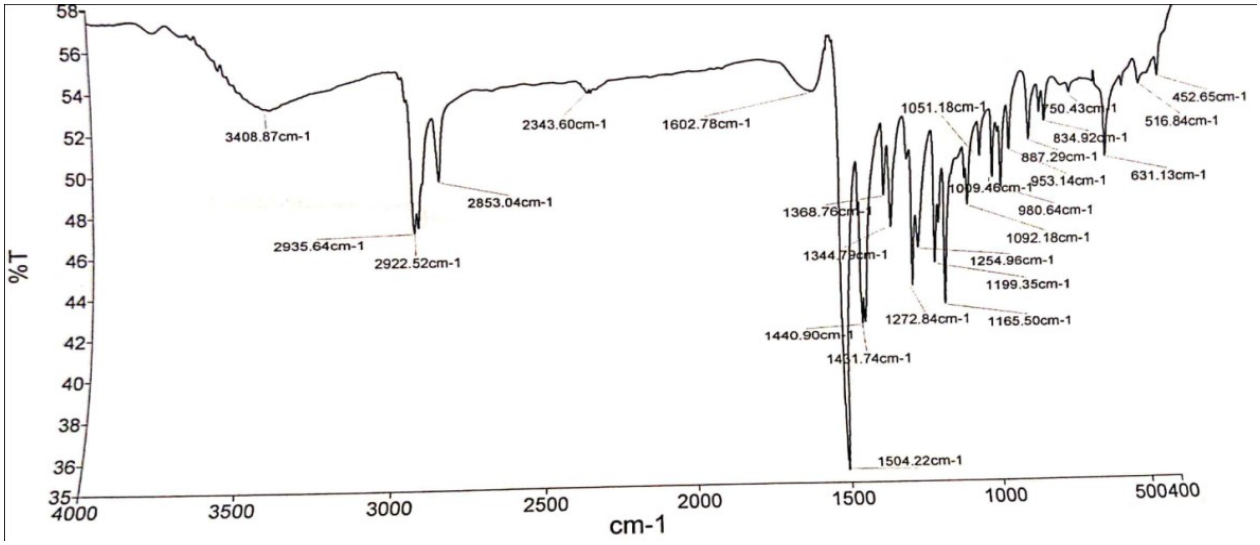

Supplementary Fig. 3: IR spectrum of $[Cu(acdt)_2]$ (**2**)

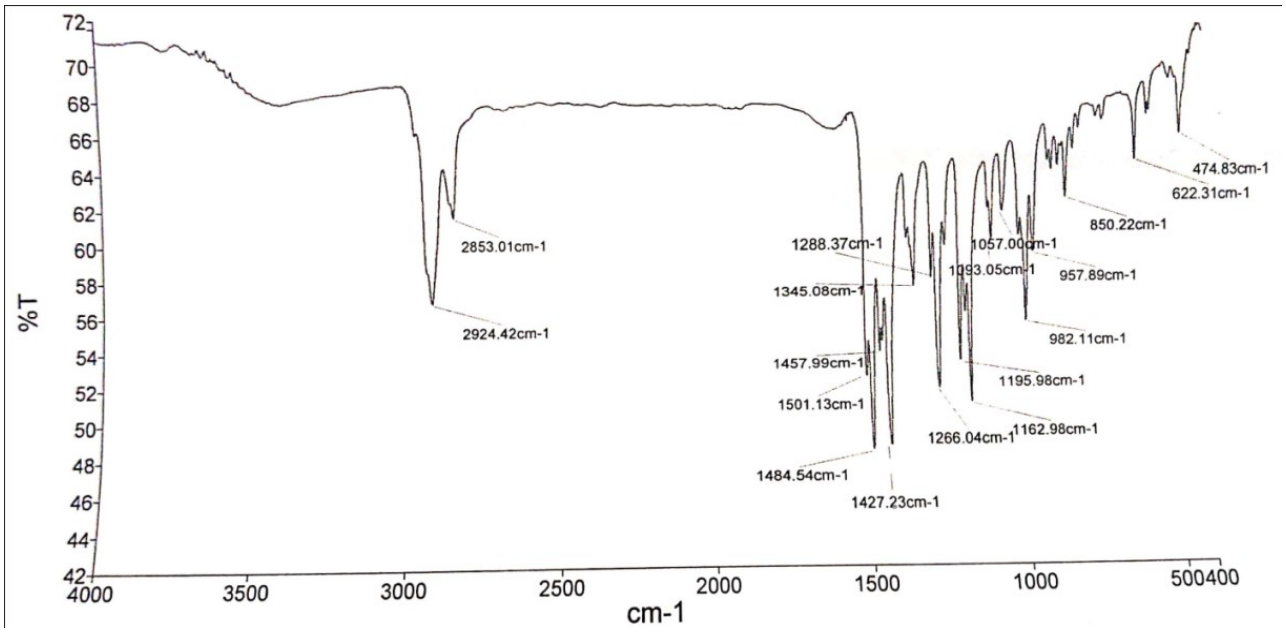

Supplementary Fig. 4: IR spectrum of $[Zn_2(\mu_2\text{-acdt})_2(acdt)_2]$ (**3**)

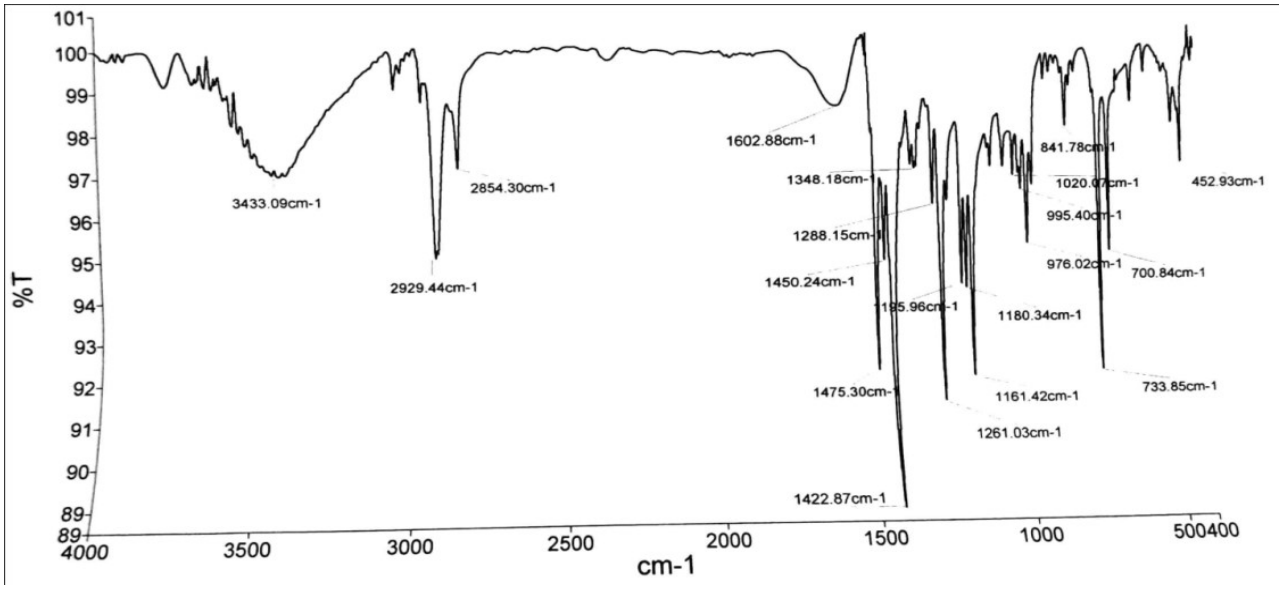

Supplementary Fig. 5: IR spectrum of [PhHg(acdt)] (**4**)

3. NMR Spectra of Ligand and its Complexes

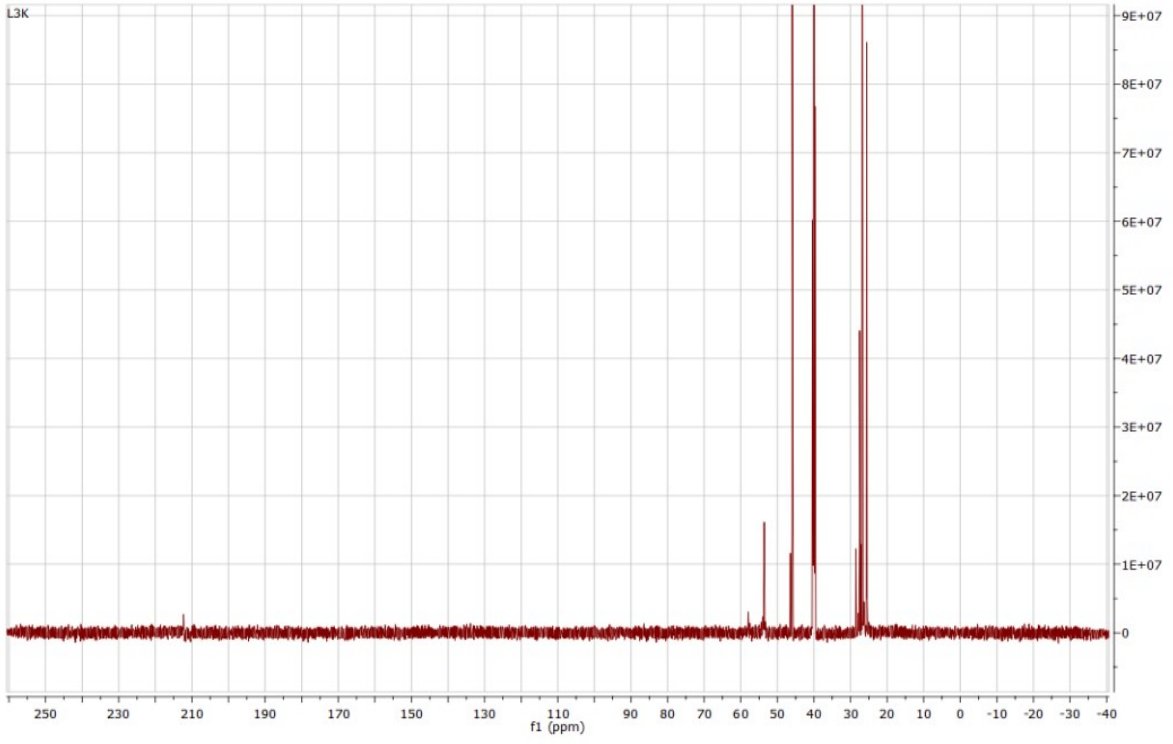

Supplementary Fig. 6: ^{13}C NMR spectrum of ligand (acdt)

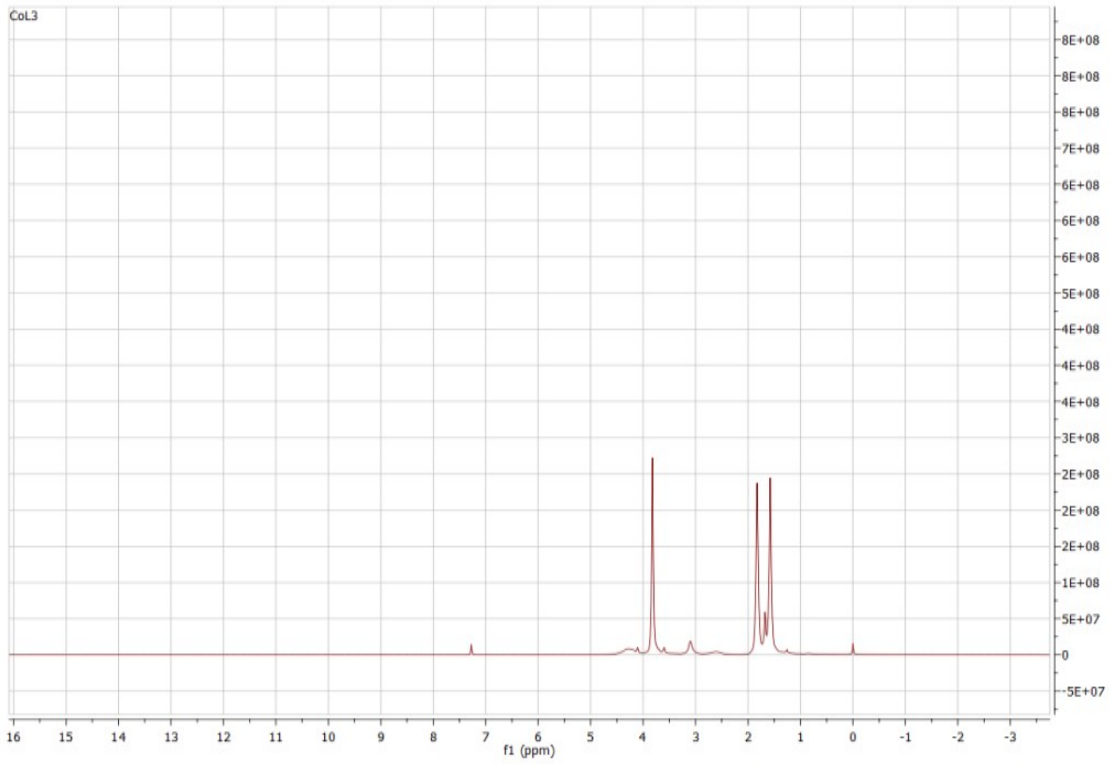

Supplementary Fig. 7: ^{1}H NMR spectrum of $[Co(acdt)_3]\cdot CHCl_3$ (**1**)

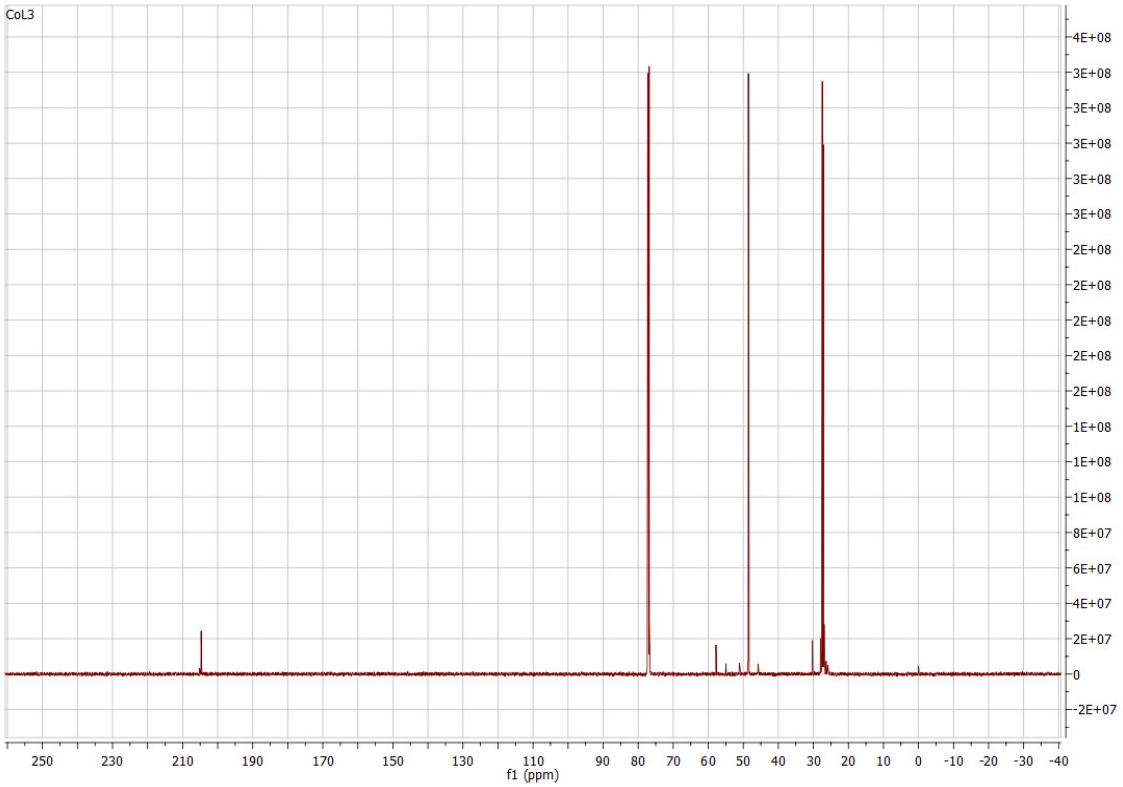

Supplementary Fig. 8: ^{13}C NMR spectrum of $[Co(acdt)_3]\cdot CHCl_3$ (**1**)

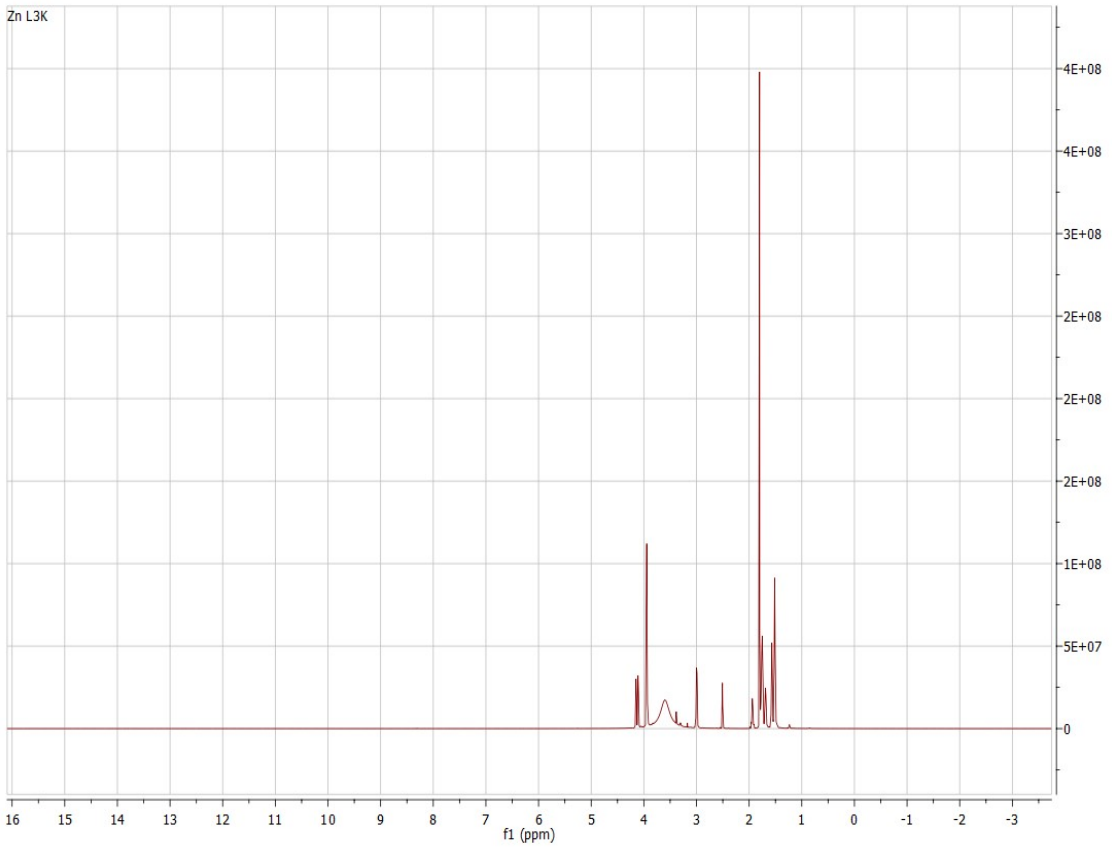

Supplementary Fig. 9: ^{1}H NMR spectrum of $[Zn_2(\mu_2\text{-acdt})_2(acdt)_2]$ (**3**)

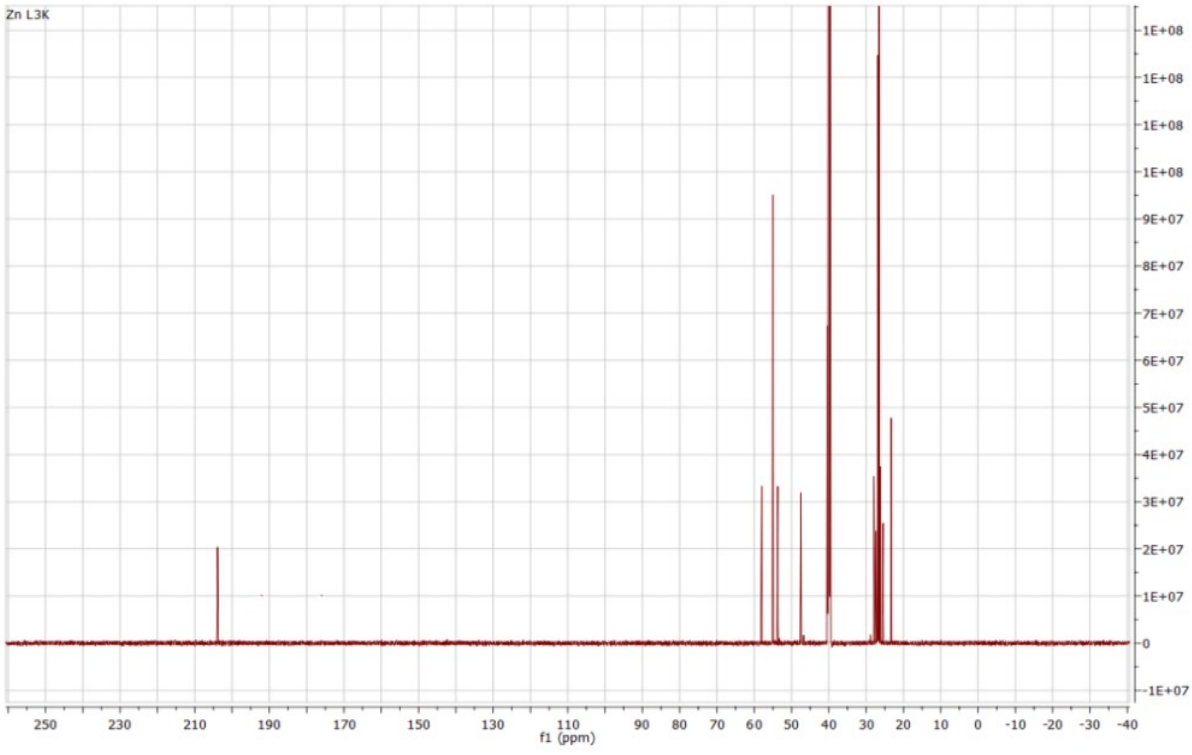

Supplementary Fig. 10: ^{13}C NMR spectrum of $[Zn_2(\mu_2\text{-acdt})_2(acdt)_2]$ (**3**)

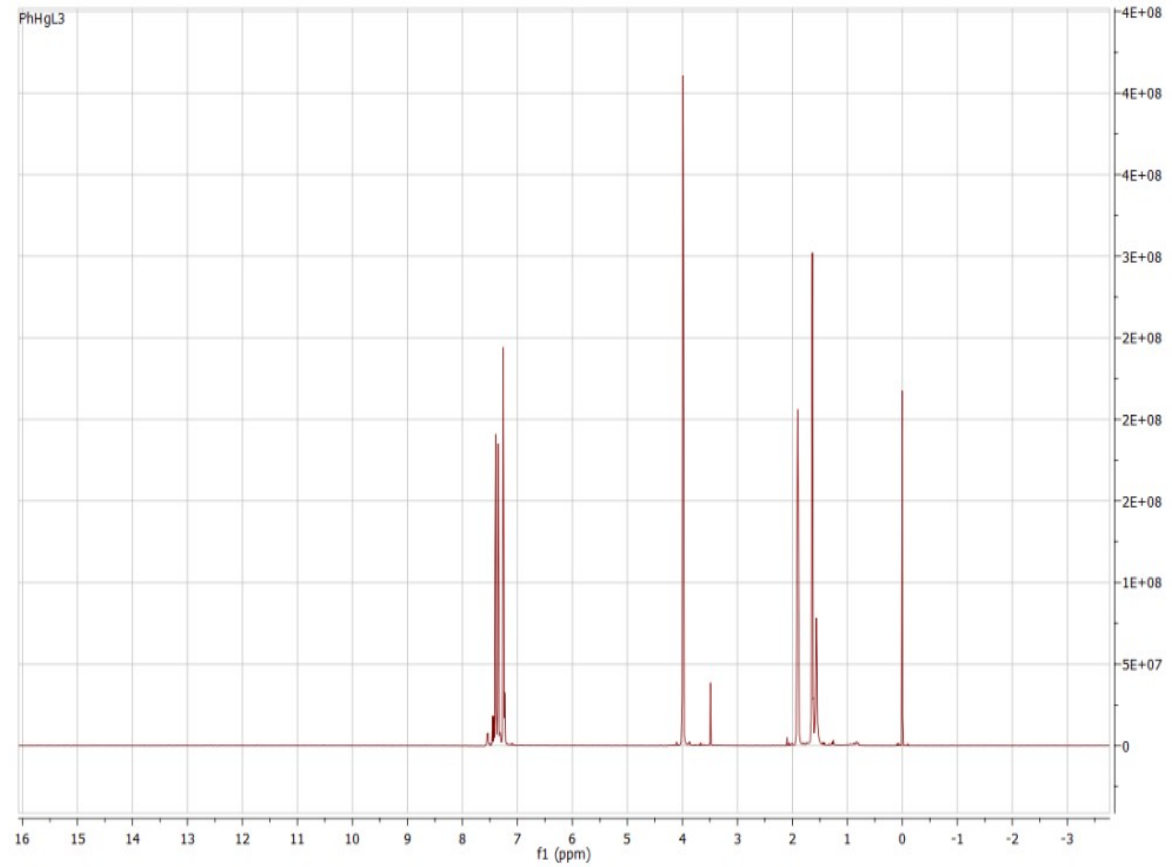

Supplementary Fig.11: ^{1}H NMR spectrum of [PhHg(acdt)] (**4**)

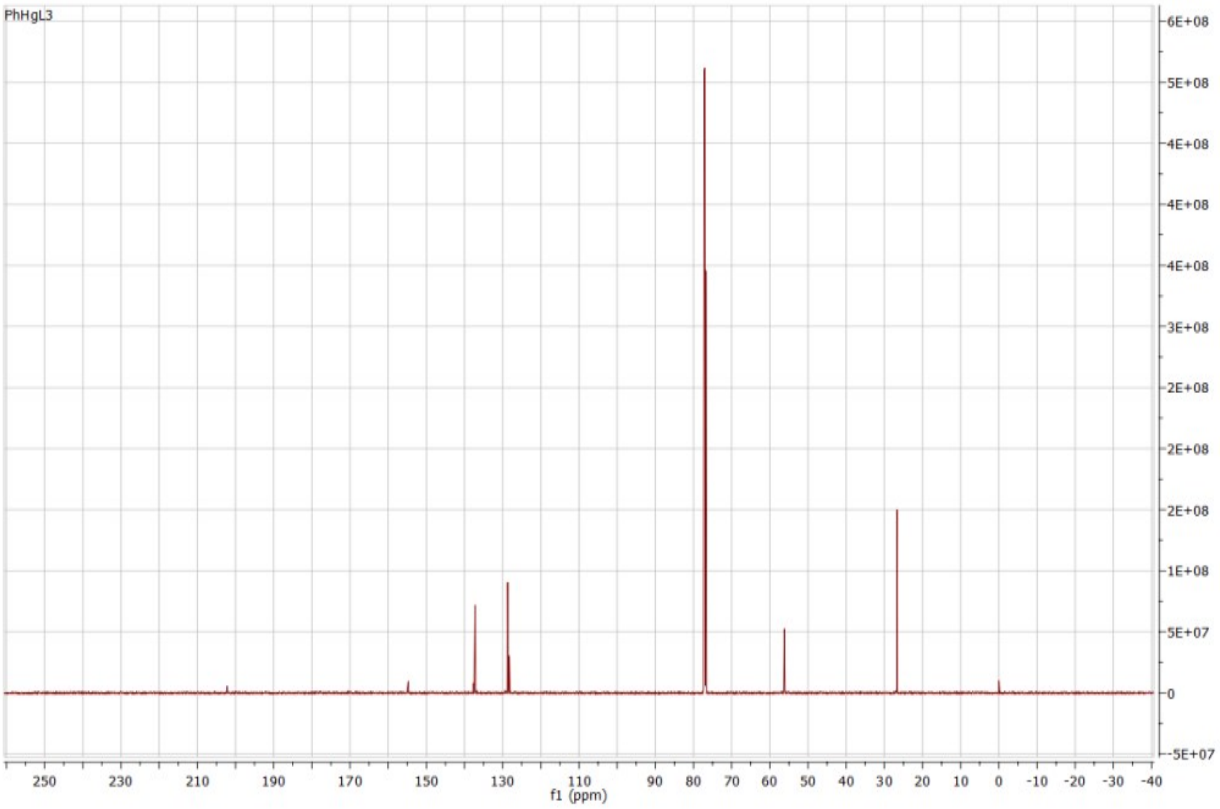

Supplementary Fig. 12: ^{13}C NMR spectrum of [PhHg(acdt)] (**4**)

4. Electronic spectra

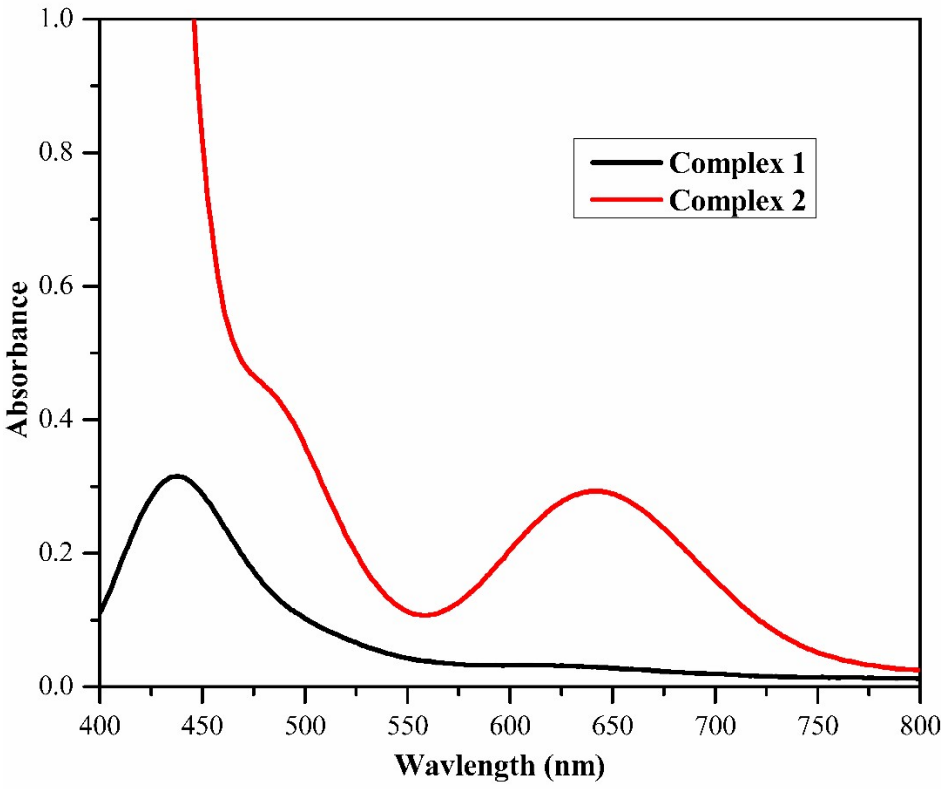

Supplementary Fig. 13: d-d Transition spectra of complexes **1** and **2** at 10^{-3} M in DMSO.

3. X-ray Crystallography

Crystals suitable for X-ray analyses of complexes 1-4 were grown at room temperature. The Single crystal data were collected on Rigaku Oxford Gemini diffractometer equipped with a CrysAlisPro CCD software using a graphite mono-chromated Mo Kα (λ= 0.71073 Å) radiation source at 296 K. A multi-scan absorption correction was solved by direct methods (SHELXL-08) and refined against all data by full matrix least-square on F^2 using anisotropic displacement parameters for all non-hydrogen atoms. All the hydrogen atoms were included in the refinement at geometrically ideal positions and refined with the riding model [9]. The MERCURY package and ORTEP-3 for windows program were used for generating the structures [10, 11].

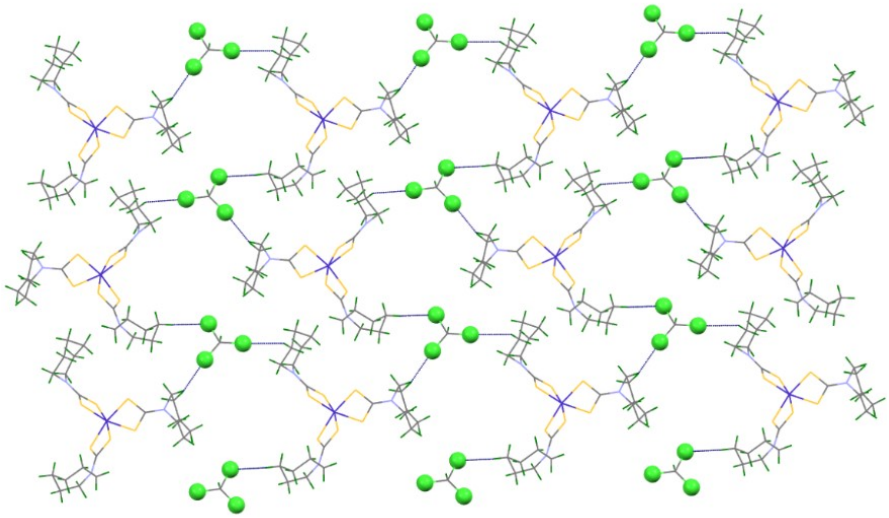

Supplementary Fig. 14: C–H···Cl hydrogen bonding interactions leading to a supramolecular architecture in complex **1**.

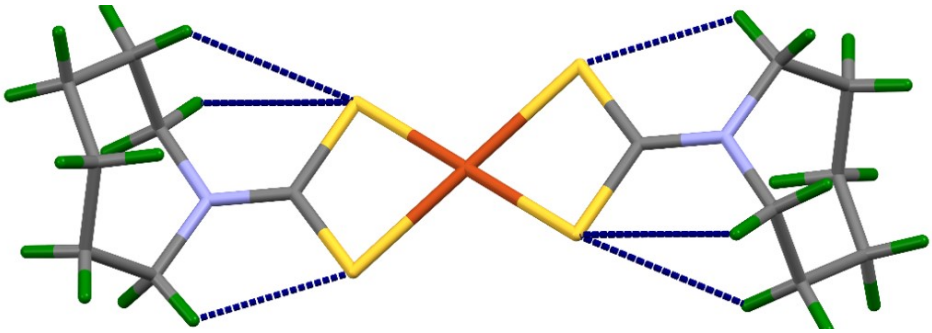

Supplementary Fig. 15: IntramolecularC–H···S hydrogen bonding interactions in complex **2**

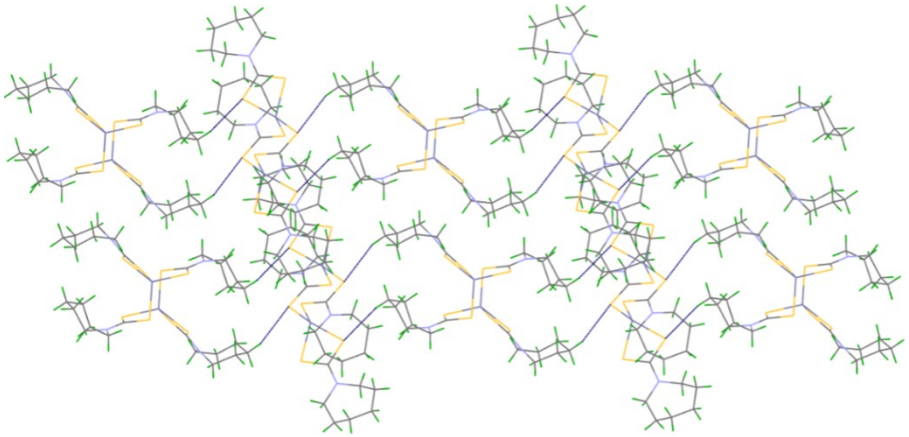

Supplementary Fig.16: C–H···S intermolecular hydrogen bonding interactions leading to a supramolecular architecture in complex **3**.

Supplementary Table 1: Selected bond distances and angles for **complex 1**

Bond length (Å)		**Bond angle (°)**	
Co(1)– S(2)	2.2782(19)	S(3)– Co(1) – S(2)	96.08(7)
Co(1)– S(3)	2.2775(19)	S(4)– Co(1)– S(2)	76.51(7)
Co(1)– S(4)	2.2618(19)	S(4)–Co(1)– S(3)	96.65(8)
Co(1)– S(5)	2.277(2)	S(4) – Co(1) – S(5)	92.58(7)
Co(1)– S(6)	2.2732(19)	S(5)– Co(1)– S(2)	94.18(7)
Co(1)– S(7)	2.2587(19)	S(6) – Co(1)– S(3)	95.32(7)
N(9)– C(15)	1.331(9)	S(6) – Co(1)–S(5)	76.53(7)
C(7)– S(6)	1.716(7)	S(7) – Co(1) – S(4)	93.22(8)
C(7)– S(5)	1.704(7)	C(15) – S(2) – Co(1)	85.9(3)
C(8)– S(7)	1.720(7)	C(7) – N(C) – C(1)	118.0(10)
C(8)– S(3)	1.710(7)	S(7) –Co(1) – S(6)	95.25(8)
C(15)– S(2)	1.701(7)	C(8) –S(3) – Co(1)	85.9(2)
C(15)– S(4)	1.714(7)	C(15) –S(4) – Co(1)	86.2(2)

Supplementary Table 2: Selected bond distances and angles for complex $[Cu(acdt)_2]$ (**2**)

Bond length (Å)		**Bond angle (°)**	
Cu(1) – S(1)	2.2893(4)	S(1) – Cu(1) – S(2)	77.592(13)
Cu(1) – S2	2.3134(4)	S(1) – Cu(1) – S(2)	102.408(13)
S(1) – C(1)	1.7285(14)	S(2) – Cu(1) – S(2)	179.999(1)
S(2) – C(1)	1.7256(14)	C(1) – S(1) – Cu(1)	84.75(5)
N(1) – C(1)	1.3224(18)	C(1) – S(2) – Cu(1)	84.07(5)
N(1) – C(2)	1.4791(19)	N(1)– C(1) – S(1)	123.08(10)
N(1) – C(7)	1.4685(19)	C(7)– N(1) – C(2)	115.98(12)

Supplementary Table 3: Selected interatomic distances and angles for $[Zn_2(\mu_2\text{-acdt})_2(acdt)_2]$ (**3**)

Bond length (Å)		**Bond angle (°)**	
Zn(1)– S(4)	2.3495(8)	S(4) –Zn(1)–S(3)	104.39(3)
Zn(1) –S(3)	2.3683(8)	S(4) –Zn(1) –S(1)	107.98(3)
Zn(1)– S(2)	2.3403(8)	S(2)– Zn(1) –S(3)	123.71(3)
Zn(1)– S(1)	2.4561(8)	S(3) –Zn(1) –S(1)	111.48(3)
S(4)– C(8)	1.716(2)	S(2)– Zn(1) –S(1)	75.64(3)
S(3) –C(8)	1.755(3)	C(8) –S(4) –Zn(1)	97.21(9)
N(2) –C(8)	1.326(3)	C(8)– S(3) –Zn(1)	102.32(8)
N(2) –C(9)	1.474(4)	C(1)– S(1) –Zn(1)	82.21(9)

Supplementary Table 4: Selected interatomic distances and angles for **[PhHg(acdt)] (4)**

Bond length (Å)		**Bond angle (°)**	
Hg(1)– C(8)	2.094(7)	C(8) – Hg(1) – S(2)	167.1(3)
S(1) – Hg(1)	2.829(4)	C(1) – S(2) – Hg(1)	92.37(18)
S(2) – Hg(1)	2.383(6)		
S(1) – C(1)	1.707(4)	C(1) – S(1) – Hg(1)	79.1(2)
S(2) – C(1)	1.751(5)	C(1) – N(1) – C(7)	121.4(4)
N(1) – C(1)	1.327(6)	C(9) – C(8) – Hg(1)	117.2(4)
N(1) – C(7)	1.478(6)	S(1) – C(1) – S(2)	119.3(3)
C(8) – C(9)	1.390(7)	N(1) – C(1) – S(2)	117.7(3)

References

[1] A. Verma, P. Gupta, N. Rai, R. K. Tiwari, A. Kumar, P. Salvi, S. C. Kamble, S. K. Singh, V. Gautam, *Journal of Fungi* **2022**, *8*(3), 285.

[2] N. Rai, P. K. Keshri, P. Gupta, A. Verma, S. C. Kamble, S. K. Singh, V. Gautam, *PLoS One* **2022**, *17*(3), e0264673.

[3] P. Gupta, N. Rai, A. Verma, D. Saikia, S. P. Singh, R. Kumar, S. K. Singh, D. Kumar, V. Gautam, *ACS omega* **2022**, *7*(50), 46653-46673.

[4] N. Rai, P. Gupta, A. Verma, R. K. Tiwari, P. Madhukar, S. C. Kamble, A. Kumar, R. Kumar, S. K. Singh, V. Gautam, *ACS omega* **2023**, *8*(4), 3768-3784.

[5] N. Rai, P. Gupta, A. Verma, S. K. Singh, V. Gautam, *BioFactors* **2023**, *49*(3), 663-683.

[6] A. Verma, N. Rai, P. Gupta, S. Singh, H. Tiwari, S. B. Chauhan, V. Kailashiya, V. Gautam, *Environmental Toxicology* **2023**, *38*(10), 2509-2523.

[7] P. Gupta, S. Singh, N. Rai, A. Verma, H. Tiwari, S. C. Kamble, H. K. Gautam, V. Gautam, *RSC advances* **2024**, *14*(6), 4074-4088.

[8] N. Rai, V. Kailashiya, V. Gautam, *ACS Pharmacology Translational Science* **2023**, *7*(1), 97-109.

[9] G. M. Sheldrick, *ActaCrystallogr. Section A*, 2008, 64, 112-122.

[10] C. F. Macrae, I.J. Bruno, J.A. Chisholm, P.R. Edgington, P. McCabe, E. Pidcock, L. Rodriguez-Monge, R. Taylor, J. van de Streek and P.A. Wood, J. Appl. Cryst., 2008, 41, 466-470.

[11] L. J. Farrugia, J. Appl. Cryst., 2012, 45, 849-854.